Journal of Medicinal Chemistry

Article

Cite This: J. Med. Chem. 2019, 62, 4456−4466

pubs.acs.org/jmc

Identification of Three-Way DNA Junction Ligands through Screening of Chemical Libraries and Validation by Complementary in Vitro Assays

Katerina Duskova,[†] Jérémy Lamarche,[†] Souheila Amor,[‡] Coralie Caron,[§,∥] Nicolas Queyriaux,[⊥] Marie Gaschard,[#] Marie-José Penouilh,[▽] Guillaume de Robillard,[†] Dominique Delmas,[‡] Charles H. Devillers,[†] Anton Granzhan,[§,∥] Marie-Paule Teulade-Fichou,[§,∥] Murielle Chavarot-Kerlidou,[⊥] Bruno Therrien,[#] Sébastien Britton,[○] and David Monchaud*[,†]

[†]Institut de Chimie Moléculaire (ICMUB), CNRS UMR6302, UBFC, 21078 Dijon, France

[‡]Lipids, Nutrition & Cancers (LNC), INSERM U1321, UBFC, 21000 Dijon, France

[§]Institut Curie, PSL Research University, CNRS UMR9187, INSERM U1196, 91405 Orsay, France

[∥]Université Paris-Sud, Université Paris Saclay, 91405 Orsay, France

[⊥]Laboratoire de Chimie et Biologie des Métaux, Université Grenoble Alpes, CNRS UMR5249, CEA, 38054 Grenoble, France

[#]Institut de Chimie, Université de Neuchâtel, CH-2000 Neuchatel, Switzerland

[▽]Pôle Chimie Moléculaire (PACSMUB), Faculté des Sciences Mirande, UBFC, 21078 Dijon, France

[○]Institut de Pharmacologie et de Biologie Structurale, IPBS, CNRS UMR5089, Université de Toulouse, UPS, équipe labellisée la Ligue Contre le Cancer, 31077 Toulouse, France

Supporting Information

ABSTRACT: The human genome is replete with repetitive DNA sequences that can fold into thermodynamically stable secondary structures such as hairpins and quadruplexes. Cellular enzymes exist to cope with these structures whose stable accumulation would result in DNA damage through interference with DNA transactions such as transcription and replication. Therefore, the chemical stabilization of secondary DNA structures offers an attractive way to foster DNA transaction-associated damages to trigger cell death in proliferating cancer cells. While much emphasis has been recently given to DNA quadruplexes, we focused here on three-way DNA junctions (TWJ) and report on a strategy to identify TWJ-targeting agents through a combination of in vitro techniques (TWJ-screen, polyacrylamide gel electrophoresis, fluorescence resonance energy transfer-melting, electrospray ionization mass spectrometry, dialysis equilibrium, and sulforhodamine B assays). We designed a complete workflow and screened 1200 compounds to identify promising TWJ ligands selected on stringent criteria in terms of TWJ-folding ability, affinity, and selectivity.

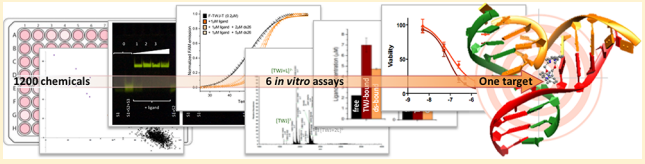

INTRODUCTION

DNA transactions (replication and transcription) are finely orchestrated cellular processes that are frequently challenged by situations of crisis notably when dealing with damaged DNA or secondary structures or in situations of nucleotide pool shortage or imbalance, which can result in DNA and RNA polymerase stalling.[1,2] If persistent, these polymerase arrests activate the DNA damage response that includes DNA repair mechanisms and that dictates cell tolerance and survival.[3,4] Crisis inducers can lead to genomic instability and eventually to cell death if DNA repair is unsuccessful or unfaithful or generates toxic products. Sources of such situations can be endogenous (e.g., stochastic nucleotide misincorporation, reactive oxygen species-promoted lesions) or exogenous (e.g., irradiation, genotoxic compounds).[5,6]

Several anticancer therapies rely on genotoxic chemicals that trigger covalent DNA damages including cross-links (e.g., cisplatin), alkylated bases (e.g., temozolomide), or trapped topoisomerase I and II complexes (e.g., camptothecin analogues and etoposide).[7,8] An alternative approach would be to consider chemicals capable of stabilizing DNA secondary structures that might arise during DNA transactions.[9,10] Repeated DNA sequences are indeed prone to fold into higher-order structures in response to the torsional stress provoked by the progression of polymerases. These secondary structures (i.e., hairpin, G-quadruplex, R-loop, DNA junction), whose nature depends on the sequences involved (i.e., direct or inverted tandem repeats), represent topological obstacles the cellular machinery must cope with efficiently to proceed, mostly through the dedicated helicases.[11] Stabilizing these structures by chemicals thus represents an innovative way to

Received: December 18, 2018
Published: April 3, 2019

DOI: 10.1021/acs.jmedchem.8b01978
J. Med. Chem. 2019, 62, 4456−4466

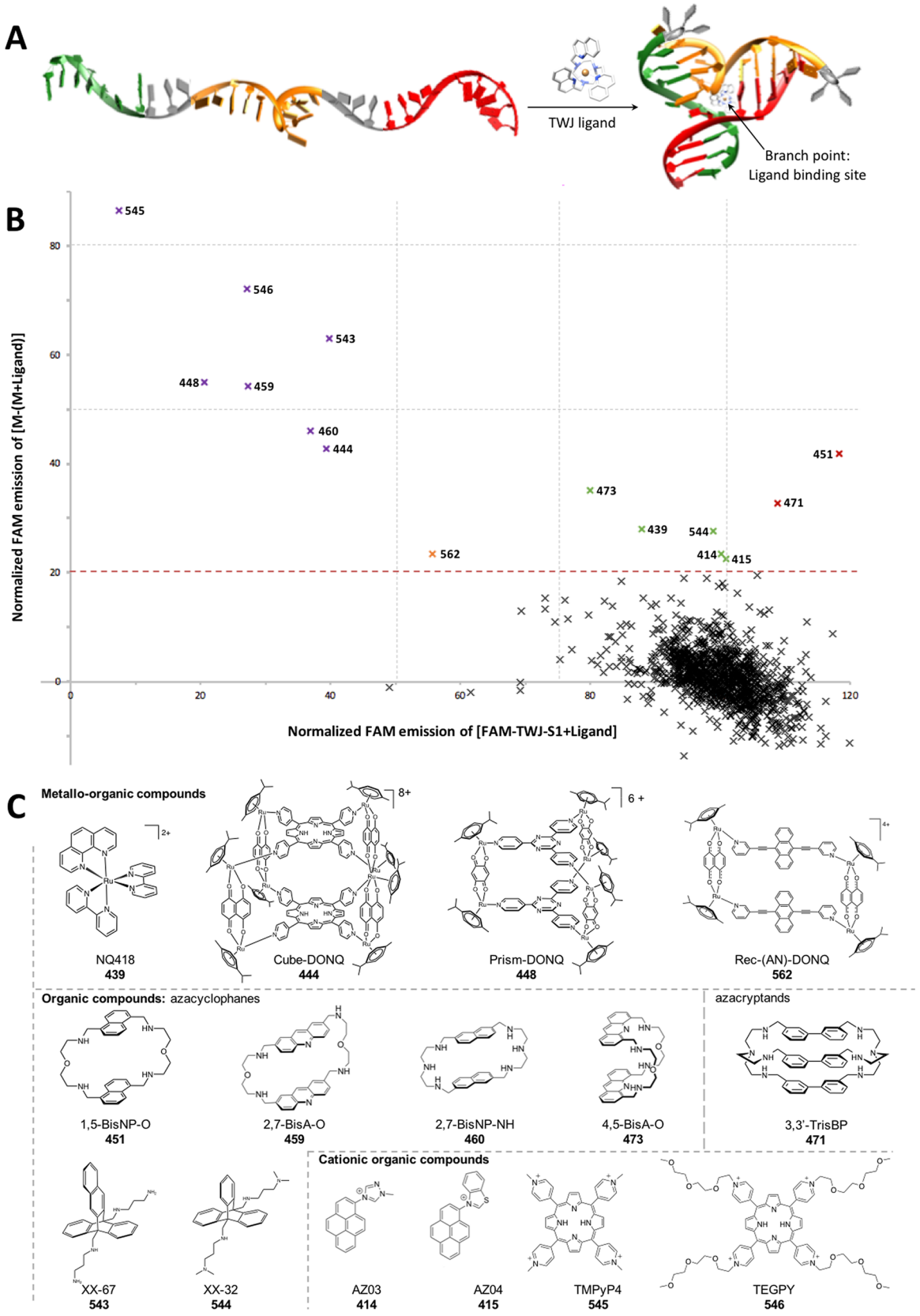

Figure 1. (A) Schematic representation of the folding of a TWJ structure. (B) TWJ-screen results of a library of 1200 compounds, expressed as the % of quenched FAM fluorescence of the three strands' mixture (M) in the presence of 5 mol equiv candidate (i.e., M−(M + ligand), *Y*-axis) as a function of the % of FAM-TWJ-S1 fluorescence measured in the presence of 5 mol equiv candidate (i.e., FAM-TWJ-S1 + ligand, *X*-axis). Experiments performed with 0.2 μM DNA, without or with 1.0 μM candidates, in 10 mM lithium cacodylate plus 10 mM KCl/90 mM LiCl, pH 7.2 at 37 °C for 1 h. (C) Chemical structures of the top 15 ligands identified through TWJ-screen evaluation.

DOI: 10.1021/acs.jmedchem.8b01978
J. Med. Chem. 2019, 62, 4456−4466

Table 1. Top TWJ Ligand Selection on the Basis of TWJ-Screen, PAGE, and FRET-Melting Assays

	TWJ-Screen[a]		PAGE[c]	FRET-melting assay			
ID	$NFI_{M-[M+ligand]}$ (%)	$NFI_{[S1+ligand]}$[b]	cplx.	$\Delta T_{1/2}$ (°C)	$\Delta T_{1/2,15eq.,\ ds26}$	$\Delta T_{1/2,50eq.,\ ds26}$	$^{FRET}S_{50eq.,\ ds26}$[d]
545	86	8% (-)	nc	22.5	12.0	8.0 °C	35% (-)
546	72	27% (+)	nc	11.0	7.0 °C	4.0 °C	36% (-)
543	63	40% (++)	-	0.8	nd	nd	nd
448	55	21% (+)	nc	15.8	8.7 °C	8.1 °C	51% (+)
459	54	27% (+)	nc	23.0	20.4 °C	17.1 °C	84% (+++)
460	46	37% (++)	+	4.2	nd[e]	nd	nd
444	43	39% (++)	+	4.9	nd	nd	nd
451	42	118% (++++)	+	10.4	8.9 °C	8.5 °C	82% (+++)
473	35	80% (+++)	nc	11.6	5.5 °C	4.6 °C	39% (-)
471	33	109% (++++)	+	17.5	16.6 °C	15.9 °C	91% (+++)
439	28	88% (+++)	-	1.8	nd	nd	nd
544	27	100% (++++)	-	0.6	nd	nd	nd
415	23	100% (++++)	-	0	nd	nd	nd
562	23	56% (+++)	-	2.0	nd	nd	nd
414	22	101% (+++)	-	1.5	nd	nd	nd

[a]Selected candidates with $NFI_{M-[M+ligand]}$ > 20%. [b]Interaction with the FAM label: "-" for $NFI_{[S1+ligand]}$ < 10%, "+" for $NFI_{[S1+ligand]}$ = 10−30%, "++" for $NFI_{[S1+ligand]}$ = 30−50%, "+++" for $NFI_{[S1+ligand]}$ = 50−100%, and "++++" for $NFI_{[S1+ligand]}$ > 100%. [c]Qualitative PAGE analysis: "nc" for non conclusive, "-" for no detectable TWJ/ligand complex, and "+" for detectable TWJ/ligand complex. [d]Selectivity determined by FRET: "-" for ^{FRET}S < 50%, "+" for ^{FRET}S = 50−80%, and "+++" for ^{FRET}S > 80%. [e]"nd" for not determined ($\Delta T_{1/2}$ < 5 °C).

trigger cell crisis and death in cells defective for genome maintenance mechanisms.

Over the past few years, most emphasis has been given to G-quadruplexes as roadblocks to DNA transactions[12−14] but also as new and promising genetic switches to control gene expression.[15,16] Alternatively, we[17−19] and others[20−27] have invested efforts to study DNA junctions as druggable targets, chiefly three-way DNA junctions (TWJ). We recently developed the high-throughput screening (HTS) assay TWJ-screen that allows for in vitro identification of promising TWJ-interacting compounds (or TWJ ligands).[19] To be selective, ligands must interact with the structural peculiarity of the TWJ structure, that is, the branch point: this cavity, at the very heart of the structure, results from the convergence of the three duplex arms that constitute the TWJ (Figure 1A). Here, we kept on searching for new TWJ ligands evaluating 1200 candidates from three different chemical libraries. We then further investigated the TWJ-interacting properties of the best candidates via a series of complementary in vitro assays (polyacrylamide gel electrophoresis (PAGE), fluorescence resonance energy transfer (FRET)-melting, electrospray ionization mass spectrometry (ESI-MS), and equilibrium dialysis) to gain reliable insights into their affinity and selectivity for TWJ.

RESULTS AND DISCUSSION

Selection of Chemical Libraries for TWJ-Screen Evaluations. To assess whether the TWJ-screen assay is suited for screening wide collections of small-molecule candidates, we used three different chemical libraries. (i) The Pathogen Box, from Medicines for Malaria Venture:[28,29] this library, available free of charge, comprises 400 druglike molecules intended to be assayed against neglected tropical diseases including malaria, tuberculosis, toxoplasmosis, dengue, etc. Chemical structures can be found at https://www.pathogenbox.org/about-pathogen-box/composition. (ii) The Chimiothèque Nationale Essentielle (CNE, version 2017):[30] this library comprises 640 compounds, either synthetic or natural products, gathered from different French laboratories under the authority of the French Chemical Library. This library is commercially available; the full list of chemicals cannot be shown due to owner restriction. (iii) The so-called ICMUB library: it comprises 160 compounds that have been assembled through national and international collaborations over the years. The full list of compounds cannot be shown due to confidentiality issues; however, the chemical structures of all identified hits are shown in Figure 1. Collectively, these three libraries represent a total of 1200 candidates, which display a very high level of chemical diversity.

Improved Version of the TWJ-Screen Assay. The TWJ-screen assay allows for quantifying the TWJ-folding ability of chemical compounds in an HTS manner.[19] This method is based on the ligand-promoted formation of a TWJ structure from a mixture of the three separated strands, two of them being labeled with fluorophores (one with fluorescein amidite, or FAM, the other one with tetramethylrhodamine, or TAMRA). The ligand-promoted TWJ formation results in the FAM and TAMRA fluorophore being in proximity, resulting in the quenching of FAM fluorescence that represents a quantitative measurement of TWJ formation. The TWJ-screen protocol was slightly adapted to screen wider chemical libraries: the initial protocol was performed at room temperature (i.e., in a 20−25 °C range), making the temperature the only parameter left uncontrolled. For improving its reproducibility, the TWJ-screen was here implemented at a fixed temperature of 37 °C. This higher temperature was selected since it allowed for improving the reproducibility of the assay—lessening the unassisted assembly of the three separated strands into a TWJ structure (vide infra)—and for selecting candidates in a more stringent manner, given that they have to fold and interact with TWJ in less-favorable thermal conditions. We screened approximately 60 candidates/day using the otherwise initially described conditions: in 100 μL (final volume) of buffered solution (10 mM lithium cacodylate buffer, pH 7.2, supplemented with 10 mM KCl/90 mM LiCl, or CacoK) was introduced 0.2 μM of the three strands initially described by Leontis et al.[31] and further studied by Brabec et al. for their ability to assemble into a TWJ

DOI: 10.1021/acs.jmedchem.8b01978
J. Med. Chem. 2019, 62, 4456−4466

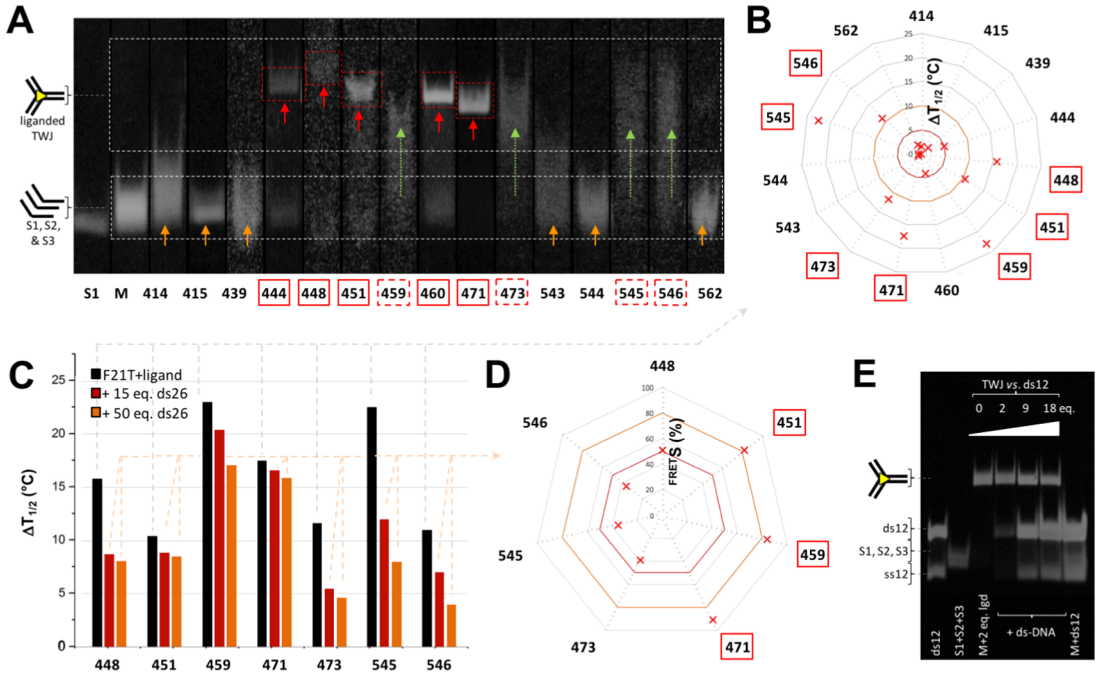

Figure 2. (A) PAGE analysis performed with TWJ-S1 (5.0 μM) and M (5.0 μM) in the absence and presence of the top 15 ligands (5 mol equiv) in TBE buffer + 100 mM NaCl, pH 8.3, at 4 °C for 1 h (gels were poststained with SybrGold; multiple gels assembled in a single image) (B–D) FRET-melting experiments performed with F-TWJ-T and the top 15 ligands in either a comparative (B, C) or a competitive manner (C, D, i.e., in the presence of increasing amounts of ds26 (up to 50 mol equiv)) expressed as $\Delta T_{1/2}$ values (in °C). Best candidates ($\Delta T_{1/2}$ > 10 °C, (B) and ^{FRET}S > 80% in the presence of 50 mol equiv ds26, (D)) are highlighted in red. Experiments performed with 0.2 μM DNA, without or with 1.0 μM candidates, with or without 3 and 10 μM ds26, in 10 mM lithium cacodylate plus 10 mM KCl/90 mM LiCl, pH 7.2, between 25 and 90 °C. (E) PAGE analysis of competitive experiments performed with TWJ strands, **471** (2 mol equiv), and increasing amounts of ds12 (up to 18 mol equiv) in TBE buffer + 100 mM NaCl, pH 8.3, at 4 °C for 45 min (gels are poststained with SybrGold for visualizing ds12 and unfolded ds12, i.e., ss12).

stable only upon interaction with ad hoc ligands,[22] that is, FAM-TWJ-S1 (FAM-d[$^{5'}$CG$_2$A$_2$CG$_2$CACTCG$^{3'}$]), TWJ-S2 (d[$^{5'}$CGAGTGCAGCGTG$_2^{3'}$]), and TWJ-S3-TAMRA (d-[$^{5'}$C$_2$ACGCTCGT$_2$C$_2$G$^{3'}$]-TAMRA). Then, 5 mol equiv (i.e., 1.0 μM) of candidate were introduced (except in control wells, vide infra) as triplicates. The microplate preparation is completed with six control wells, that is, three wells with FAM-TWJ-S1 alone (to define the 100% FAM emission) and three wells with the three separated strands (a mixture termed M) to verify the lack of spontaneous TWJ folding. The microplate is centrifuged (30 s) and then gently stirred for 1 h at 37 °C prior to fluorescence reading. The proficiency of candidates to shift the equilibrium toward the folded TWJ is quantified by comparing the normalized FAM intensity (NFI) of FAM-TWJ-S1 alone (defined as 100%) versus [FAM-TWJ-S1 + ligand] (for discarding unwarranted compound's interaction with S1) on the one hand and the NFI of the mixture M vs [M + ligand] (that quantifies the TWJ folding per se) on the other hand. Collected results are shown in Figure 1B and Table 1. The vast majority of the 1200 compounds screened were found ineffective ($NFI_{M-[M+ligand]}$ → 0%, $NFI_{[FAM-TWJ-S1+ligand]}$ → 100%), but 15 candidates emerged, displaying $NFI_{M-[M+ligand]}$ values > 20% (red dashed line, Figure 1B) (the complete TWJ-screen results are provided in the Supporting Information). These ligands, compounds **414**, **415**, **439**, **444**, **448**, **451**, **459**, **460**, **471**, **473**, **543**, **544**, **545**, **546**, and **562**, illustrated all possible scenarios, from candidates that display a good ability to fold TWJ without interacting with the FAM label (flagged as "++++" in Table 1; e.g., **451**, with $NFI_{M-[M+ligand]}$ = 42% and $NFI_{[FAM-TWJ-S1+ligand]}$ > 100%) to compounds with very high $NFI_{M-[M+ligand]}$ and very strong interaction with the FAM label (flagged as "-" in Table 1; e.g., **545**, with $NFI_{M-[M+ligand]}$ = 86% and $NFI_{[FAM-TWJ-S1+ligand]}$ = 8%). The TWJ-screen assay thus allowed for sorting molecules in a very stringent manner. The chemical structures of the 15 candidates are shown in Figure 1C. It is unsurprising to find previously identified hits,[18,19] including the azacyclophanes 1,5-BisNP-O (**451**), 2,7-BisA-O (**459**), 2,7-Bis-NP-NH (**460**), and 4,5-BisA-O (**473**) and the azacryptand 3,3′-TrisBP (**471**)[32] and the metallacages Cube-DONQ (**444**) and Prism-DONQ (**448**).[33] We also identified new candidates (all from the ICMUB library) that all display well-defined molecular shapes and volumes: the ruthenium trisdiimine complex NQ418 (**439**); two new triptycene derivatives XX-67 (**543**) and XX-32 (**544**), whose synthesis will be described elsewhere (Granzhan et al.), structurally close to the compounds previously studied by Chenoweth and co-workers;[25,26] and a newly reported organometallic cage Rec-(AN)-DONQ (**562**).[34] Classical DNA intercalators are also identified, notably two porphyrins, TMPyP4 (**545**)[35] and TEGPy (**546**),[36] and two cationic pyrene derivatives, AZ03 (**414**) and AZ04 (**415**),[37] owing to their innate ability to interact with negatively charged nucleic acids.

Confirming the TWJ-Folding Capability via Non-denaturing PAGE Analyses. To further investigate the intrinsic quality of the 15 identified candidates, their TWJ-folding capabilities were subsequently investigated by non-denaturing PAGE analysis according to the methodology described by Brabec et al.[22] We used the same TWJ-forming strands, TWJ-S1, TWJ-S2, and TWJ-S3 (without fluorescent labels). The obtained gels (15% polyacrylamide, 5 μM DNA

DOI: 10.1021/acs.jmedchem.8b01978
J. Med. Chem. 2019, 62, 4456–4466

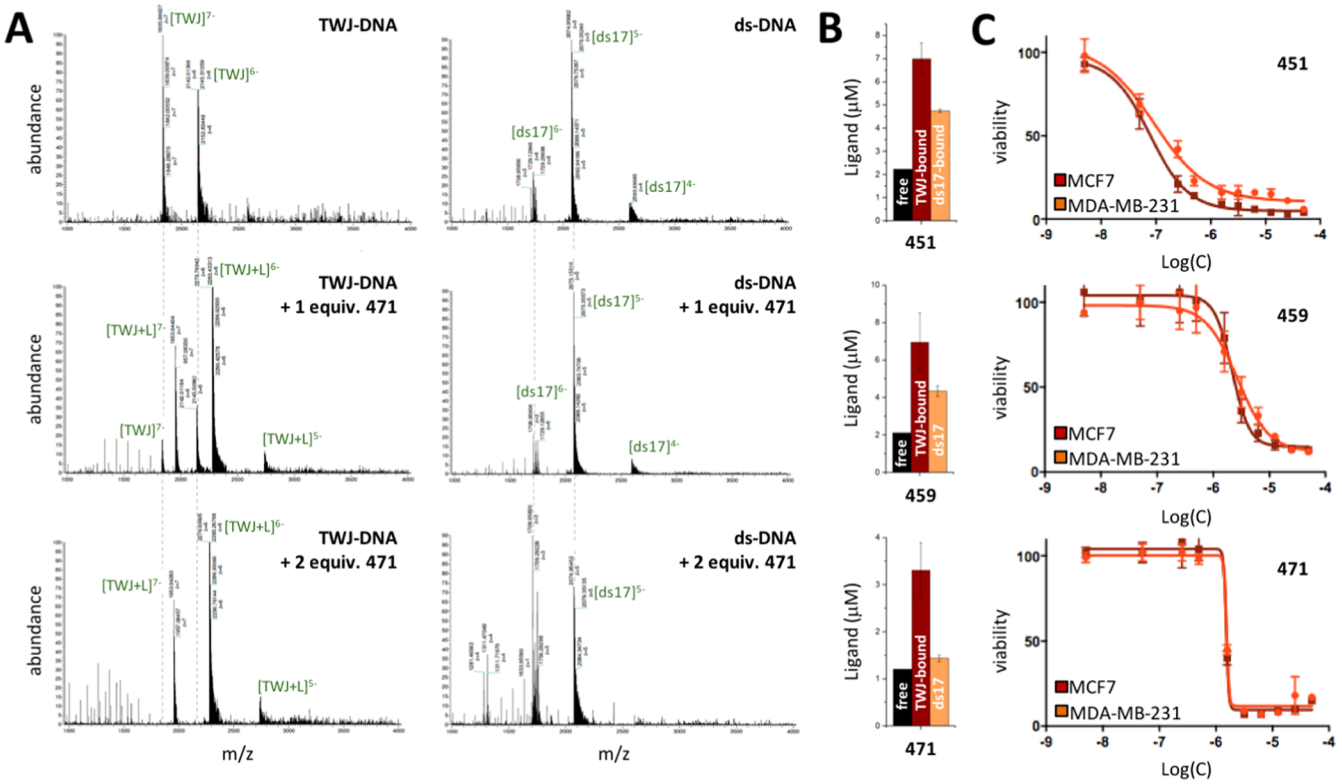

Figure 3. (A) ESI-MS profiles of the association of TWJ (left panels) or ds17 (right panels) with increasing amounts (0, 1, and 2 mol equiv) of **471**. Experiments performed with 5.0 μM DNA, without or with 5.0 or 10 μM ligand, in 100 mM ammonium acetate, pH 7.2, after 1 h equilibration at 25 °C. (B) Equilibrium dialysis results for **451**, **459**, and **471** (black bars, free ligand; brown bar, ligand bound to TWJ; orange bar, ligand bound to ds17). Experiments performed with 75 μM DNA (base pairs), without or with 2 μM ligand, in sodium phosphate + 100 mM NaCl, pH 7.2, after 24 h equilibration at 25 °C. (C) Viability profiles obtained via the sulforhodamine B (SRB) assay with **451**, **459**, and **471** after 72 h incubation (37 °C, Dulbecco's modified Eagle's medium (DMEM)) with MCF7 (brow line) and MDA-MB-231 (orange line) cells.

loading/well), presented in Figure 2A, offered a straightforward—but qualitative—reading of the TWJ-folding ability of the candidates, visualized by the difference of migration between the TWJ-S1 alone and the mixture of strands M (lower dashed rectangle) and the folded TWJ/ligand complexes, which migrate significantly more slowly (upper dashed rectangle). Five compounds were found efficient in these conditions (red arrows), i.e., **444**, **448**, **451**, **460**, and **471**; four compounds led to a smeared band (green arrows), i.e., **459**, **473**, **545**, and **546**, thus making conclusions hard to draw solely on the basis of PAGE; and six compounds were found inactive (yellow arrows), i.e., **414**, **415**, **439**, **543**, **544**, and **562**. Given that PAGE conditions are known to be challenging for noncovalent assemblies, these results underline the good TWJ-interacting properties of the five most efficient compounds.

Investigating the TWJ-Interacting Properties via the FRET-Melting Assay. We also assessed whether the 15 identified ligands interact with a prefolded TWJ structure. To this end, their ability to stabilize folded DNA junctions against thermal denaturation was evaluated by the FRET-melting assay using the doubly labeled FAM-d[$^{5'}$A(CT)$_2$(TC)$_2$G-T$_6$-C-(GA)$_2$GCGAC-T$_6$-GTCGC(AG)$_2$T$^{3'}$]-TAMRA system (FAM-TWJ-TAMRA, or F-TWJ-T).[35] Experiments were performed as follows: in 100 μL (final volume) of buffered solution (CacoK), 0.2 μM of F-TWJ-T in the absence (control wells) or presence of 5 mol equiv (i.e., 1.0 μM) ligands (as triplicates) was heated from 25 to 75 °C (1 °C per step). The melting of the DNA structure was monitored through FAM emission (quenched at low temperature due to the close proximity with TAMRA in folded TWJ and restored at elevated temperature due to the thermal unfolding of the DNA junction): the thermal stability of F-TWJ-T, expressed as its melting temperature $T_{1/2}$ (here, $T_{1/2}$ = 43.4 °C in the absence of a ligand), increased up to 66.4 °C in the presence of the best TWJ stabilizer (compound **459**, $\Delta T_{1/2}$ = 23.0 °C, Table 1). The $\Delta T_{1/2}$ values for the 15 selected compounds are reported in Figure 2B: only seven of these candidates (**448**, **451**, **459**, **471**, **473**, **545**, and **546**) imparted a significant stability ($\Delta T_{1/2}$ > 10 °C, Table 1). Compounds **444** and **460**, yet the most promising candidates by PAGE, would have been discarded on the FRET-melting result basis ($\Delta T_{1/2}$ = 4.9 and 4.2 °C, respectively); conversely, **459**, the most efficient TWJ stabilizer here, led to debatable PAGE results. This discrepancy illustrated that TWJ-screen and FRET-melting assays monitored two different processes (TWJ folding on the one hand and stabilization of folded TWJ on the other hand), thus making these two tests complementary.

The TWJ-interacting properties of these seven candidates were further investigated via competitive FRET-melting experiments to assess their TWJ selectivity over duplex DNA. Experiments were performed with F-TWJ-T, 5 mol equiv of ligand, in the absence (control wells) or presence of 15 or 50 mol equiv of a duplex competitor, here ds26 (comprising two self-complementary strands ss26 d-[^{5}CA$_2$TCG$_2$ATCGA$_2$T$_2$CGATC$_2$GAT$_2$G$^{3'}$]). The capacity of a ligand to withstand the excess of ds26 is expressed as ^{FRET}S values (^{FRET}S = ($\Delta T_{1/2}$[+ds26]/$\Delta T_{1/2}$[no ds26]) × 100, in %).

DOI: 10.1021/acs.jmedchem.8b01978
J. Med. Chem. 2019, 62, 4456−4466

Table 2. Quantification of DNA Interactions (ESI-MS and Dialysis) and Toxicity (SRB) of the Top 3 TWJ Ligands

	ESI-MS (K, M^{-1})[a]			Equilibrium dialysis (K_{app}, M^{-1})			SRB test (LD_{50}, μM)		
ID	TWJ	ds	TWJ/ds	TWJ	ds	TWJ/ds	MCF7	MDA	BJ-hTERT
451	4.7×10^7	7.5×10^4	>2-log	8.7×10^6	5.9×10^5	>1-log	0.10	0.16	0.04
459	1.9×10^9	3.1×10^4	>4-log	1.4×10^7	3.8×10^5	>1-log	4.80	2.80	1.00
471	3.9×10^6	7.5×10^3 [b]	>2-log[b]	6.0×10^6	4.7×10^4	>2-log	1.30	1.30	2.60

[a] K calculations on the basis of experiments performed with 10 μM DNA and 20 μM ligands. [b] No ds17/**471** interactions were detected at the 1:2 ratio; K_a was calculated for experiments performed at a 1:3 DNA/ligand ratio.

Results seen in Figure 2C and Table 1 indicate that only three compounds are both good stabilizers ($\Delta T_{1/2}$ > 10 °C) and selective (^{FRET}S > 80%), that is, the azacyclophanes **451** and **459** and the azacryptand **471**, making them the most promising ligands identified through this three-step selection process. These results also discarded the two porphyrins (**545** and **546**) as false positives owing to their low selectivities (^{FRET}S = 35 and 36%, respectively), which makes them prone to interact with nucleic acids irrespective of their secondary structures.

Of note, the exquisite selectivity of **471** (^{FRET}S = 91%, Table 1) was further investigated via a competitive PAGE analysis performed with an excess (2, 9, and 18 mol equiv) of duplex DNA (here ds12, comprising two self-complementary strands ss12 d[$^{5'}$CGCGA$_2$T$_2$CGCG$^{3'}$]). Results seen in Figure 2E confirmed that the TWJ-folding capability of **471** withstands the presence of competitive duplexes, thereby further demonstrating its selectivity for DNA junctions.

Collectively, these results highlight the necessity of performing TWJ-screen, PAGE, and FRET-melting evaluations in a stepwise manner to identify promising ligands on a reliable basis. In the present case, three compounds passed this series of tests successfully, namely, the macrocycles **451** and **459** (1,5-BisNP-O and 2,7-BisA-O, respectively) and the macrobicycle **471** (3,3′-TrisBP).

Quantifying the Ligand–TWJ DNA Association by ESI-MS and Equilibrium Dialysis Analyses. We next investigated further the TWJ-interacting properties of **451**, **459**, and **471** via electrospray ionization mass spectrometry (ESI-MS). This technique provides a unique opportunity to directly access both the equilibrium affinity constants (K) and the stoichiometry of the ligand–DNA association as already documented with duplex- and quadruplex DNA[38] but not yet applied to DNA junctions. Investigations were here performed with both the prefolded TWJ used for FRET-melting investigations (without fluorescent labels) and the duplex DNA ds17 (d[$^{5'}$C$_2$AGT$_2$CGTAGTA$_2$C$_3$$^{3'}$]/d-[$^{5'}G_3T_2$ACTACGA$_2CTG_2$$^{3'}$]). Measurements were performed in 80:20 (v/v) ammonium acetate buffer (100 mM, pH 7.0)/MeOH with 5 μM DNA and increasing amounts of ligands (from 0 to 2 mol equiv). Results obtained with **471** (Figure 3A; see the Supporting Information for compounds **451** and **459**) showed the exclusive formation of the 1:1 TWJ/**471** complex, regardless of the DNA/ligand ratio, and no interaction with ds17. These results highlighted a unique ligand binding site within the TWJ structure—most likely the branch point—and confirmed the exquisite TWJ selectivity of **471**. Similar experiments performed with **451** and **459** showed that the major species is the 1:1 TWJ/ligand complexes as well, along with traces of free DNA and 2:1 complexes, and also highlighted weak and random interactions with ds17 (since 1:1, 2:1, and 3:1 complexes could be detected). To further characterize and quantify these interactions, we calculated the equilibrium association constants (Table 2):[39] K values confirmed the high affinities of **451**, **459**, and **471** for TWJ (K between 3.9×10^6 and 1.9×10^9 M^{-1}) along with their excellent selectivity over duplex DNA (>2-log difference).

We next decided to confirm these results by an alternative technique, performed in solution, and selected the equilibrium dialysis (or competition dialysis) that has been already applied to a wide variety of DNA structures (single-stranded and double-stranded DNA, triplex- and quadruplex DNA)[40] but not to DNA junctions. In this experiment, both TWJ and ds17, isolated from the main solution in semipermeable chambers (200 μL at 75 μM, expressed in base pairs), were dialyzed against a solution of ligands (200 mL at 2 μM). After equilibration (24 h, 25 °C), the amount of ligand bound to each structure is quantified by fluorescence titration of the content of the dialysis chambers after leaking the ligand by 1% sodium dodecyl sulfate (SDS) treatments (versus a quantification of the ligand remaining in the dialysis solution). Results presented in Figure 3B show the preferred fixation of the ligands onto TWJ but also emphasized the better selectivity of **471** as compared to **451** and **459**. Again, we quantified these interactions through the calculations of the apparent affinity constant K_{app} (Table 2):[40] they confirmed the high affinities of **451**, **459**, and **471** for TWJ (K_{app} between 6.0×10^6 and 1.4×10^7 M^{-1}) along with their good (**451** and **459**) to excellent selectivity over duplex DNA (>2-log difference for **471**).

Preliminary Cell-Based Assays with 451, 459, and 471. After the thorough evaluation of their TWJ-interacting properties in vitro, we decided to evaluate the antiproliferative properties of **451**, **459**, and **471** against cancer cells. Their cellular activities were evaluated on two cancer cell lines, MCF7 and MDA-MB-231, which are extensively used in the study of experimental therapeutics since they represent two different classes of breast cancers: MCF7 cells are derived from a hormone-responsive cancer, expressing estrogen (ER), progesterone (PR), and glucocorticoid receptors (GRs); and MDA-MB-231 cells are representative of triple-negative breast cancers (ER$^-$, PR$^-$, and HER2$^-$ (human epidermal growth factor receptor 2)), which are typically more aggressive and challenging to cure. In addition, MCF7 and MDA-MB-231 are instrumental for the evaluation of DNA-damaging agents since they have functional and mutant p53, respectively, a critical protein controlling DNA damage checkpoints and mediating cell-cycle arrests and/or apoptosis in response to DNA damage. Viability analysis was performed here through the sulforhodamine B (SRB) test,[41,42] and the collected results were compared to the firmly established anticancer (and DNA-damaging) agent camptothecin (Figure S4).[43] To this end, cells were incubated for 72 h at 37 °C in DMEM without or with a ligand prior to fixation with a solution of trichloroacetic acid 10% (1 h at 4 °C). After supernatant removal, a solution of SRB (0.2% in 1% acetic acid) was added for 30 min before being washed (acetic acid 1%) and dried. A solution of Tris

DOI: 10.1021/acs.jmedchem.8b01978
J. Med. Chem. 2019, 62, 4456–4466

Table 3. Oligonucleotides Used in this Study

status	nature	name	sequence
labeled	TWJ	FAM-TWJ-S1	FAM-d[$^{5'}$CG$_2$A$_2$CG$_2$CACTCG$^{3'}$]
		TWJ-S3-TAMRA	d[$^{5'}$C$_2$ACGCTCGT$_2$C$_2$G$^{3'}$]-TAMRA
		F-TWJ-T	FAM-d[$^{5'}$A(CT)$_2$(TC)$_2$G-T$_6$-C(GA)$_2$GCGAC-T$_6$-GTCGC(AG)$_2$T$^{3'}$]-TAMRA
unlabeled	TWJ	TWJ-S1	d[$^{5'}$CG$_2$A$_2$CG$_2$CACTCG$^{3'}$]
		TWJ-S2	d[$^{5'}$CGAGTGCAGCGTG$_2$$^{3'}$]
		TWJ-S3	d[$^{5'}$C$_2$ACGCTCGT$_2$C$_2$G$^{3'}$]
		TWJ	d[$^{5'}$A(CT)$_2$(TC)$_2$G-T$_6$-C(GA)$_2$GCGAC-T$_6$-GTCGC(AG)$_2$T$^{3'}$]
	duplex	ds12	strand 1: d[$^{5'}$CGCGA$_2$T$_2$CGCG$^{3'}$]
			strand 2: d[$^{5'}$CGCGA$_2$T$_2$CGCG$^{3'}$]
		ds17	strand 1: d[$^{5'}$CCAGTTCGTAGTAACCC$^{3'}$]
			strand 2: d[$^{5'}$GGGTTACTACGAACTGG$^{3'}$]
		ds26	strand 1: d[$^{5'}$CAATCGGATCGAATTCGATCCGATTG$^{3'}$]
			strand 2: d[$^{5'}$GTTAGCCTAGCTTAAGCTAGGCTAAC$^{3'}$]

base (10 mM) was then added to allow for optical density (OD) reading (at 530 nm) to assess cell viability and determine the lethal dose (LD_{50}, the concentration at which 50% of the cell growth inhibition is reached).

The results (Figure 3C and Table 2) showed that the cellular activity stood in the same range for both cells lines, with higher inhibition properties for **451** (with LD_{50} = 0.10 and 0.16 μM for MCF7 and MDA-MB-231, respectively), then for **471** (LD_{50} = 1.30 and 1.30 μM) and for **459** (LD_{50} = 4.80 and 2.80 μM). In these conditions, **451** displayed a higher activity than camptothecin (with LD_{50} = 1.70 and 1.40 μM), which is here found comparable to **471**. For the sake of comparison, we also performed SRB investigations with normal fibroblasts (BJ-hTERT) as models of healthy cells.[44] As seen in Table 2, only **471** was found less toxic in BJ-hTERT than in cancer cells (2-fold difference, with LD_{50} = 1.30 and 2.60 μM for cancer cells and BJ-hTERT, respectively), making it the most promising compound from that series of ligands. To gain insights into the capacity of **471** to trigger DNA damage, we performed preliminary immunodetection studies using an antibody raised against the phosphorylated histone H2AX (so-called γH2AX), an established marker of DNA damage.[45] The pilot study was carried out with MCF7 treated with **471** and camptothecin as the control. Collected images seen in Figure S5 confirmed that the ligands triggered a marked accumulation of γH2AX foci. These preliminary data thus provide an encouraging sign for the future of this new class of noncanonical DNA structure-targeting ligands as DNA-damaging agents, and efforts are now invested to establish a firm link between cellular TWJ interaction and DNA damage.

CONCLUSIONS

Compared to normal cells, cancer cells harbor a flawed repertoire of DNA damage signaling and repair capabilities, collectively known as DNA damage response, or DDR.[1−6] Three main aspects of DDR make cancer cells different from healthy cells: (i) loss of one or more DDR pathways, (ii) increased level of replicative stress, and (iii) endogenous DNA damages.[46] These aspects thus provide a window of therapeutic opportunities for compounds that trigger or exacerbate cellular crisis states. Our approach is here focused on compounds that stabilize three-way DNA junctions (TWJ) given that these higher-order DNA structures represent topological hindrances to polymerase that can hamper proper DNA transactions (replication, transcription).[9] The TWJ ligands could thus represent a novel and promising class of crisis-inducing agents.

To identify promising TWJ ligands, we developed and report here a validation framework that comprises six complementary in vitro assays: the TWJ-screen assay, which allowed for evaluating the ability to promote the TWJ folding of 1200 compounds; a PAGE analysis, which confirms the TWJ-folding ability of the 15 identified candidates in more stringent conditions; the FRET-melting assay, which provides insights into both the TWJ-stabilizing properties and selectivity of the identified candidates; ESI-MS investigations, which further studied TWJ selectivity and gives access to a quantification (affinity constants, K_a) of the ligand−DNA association; the equilibrium dialysis, which provides an alternative quantification of the ligand−DNA binding parameters; and the SRB test, which assesses the antiproliferative activity of identified TWJ ligands against human breast cancer cells (MCF7 and MDA-MB-231).

Collectively, the wealth of data collected in the course of this study highlights the strength of our methodology to uncover TWJ ligands, with the identification of three promising compounds here, namely, **451**, **459**, and **471**, whose properties make them ideally suited to be used as prototype ligands throughout the validation chain. Exploring their use as anticancer agents will require to decipher the mechanisms underlying their antiproliferative properties. Also, our results highlight the need for screening wider chemical libraries to uncover ever more efficient TWJ ligands, and we are convinced that the framework described here is an ideal toolbox to do so. Importantly, libraries to be tested must not be focused on druglike compounds or small molecules only (like the Pathogen Box or the CNE) but must include chemicals with defined shapes and volumes, given that it appears to be a major determinant of efficient TWJ ligands. Indeed, thanks to the pioneering investigations by Hannon and co-workers performed with iron supramolecular cylinders,[20−24] we know that the privileged binding site for compounds within the TWJ structure is the branch point, a cavity that results from the convergence of three duplex arms. This cavity is hydrophobic owing to its side walls made of base pairs (here two T = A and one G≡C base pairs), thus being suited to accommodate sterically demanding ligands displaying large aromatic moieties. This was confirmed here through the unveiling of three promising candidates, the azacyclophanes **451** and **459** (1,5-BisNP-O and 2,7-BisA-O, respectively) and the azacryptand **471** (3,3′-TrisBP), all of which display well-defined three-

DOI: 10.1021/acs.jmedchem.8b01978
J. Med. Chem. 2019, 62, 4456−4466

dimensional structures and large aromatic moieties (naphthalene, acridine, and bipyridine) prone to interacting efficiently with the cavity walls. These results thus provide new perspectives on and further insights into the cellular activity of the azacyclophanes and azacryptands, which could originate in multiple dysregulated pathways (TWJ interaction as well as interactions with abasic sites and cleavage and inhibition of DNA repair).[47,48] They also contribute to expand the portfolio of DNA binders with promising anticancer properties and the panoply of DNA structure targets with high therapeutic value.

EXPERIMENTAL SECTION

Chemicals. The open access Pathogen Box comprises 400 compounds with biological activity against specific pathogenic organisms. The box is provided by the Medicines for Malaria Venture as an open access compound collection (http://www.pathogenbox.org/). The chimiothèque nationale essentielle is a collection of 640 compounds assembled by and purchased from the French National chemolibrary (http://chimiotheque-nationale.cn.cnrs.fr/). All other chemicals have been prepared according to methodologies described (with purity ≥95% as evaluated by elemental analyses or high-performance liquid chromatography−-mass spectrometry) in the corresponding references, except camptothecin (99.8% purity), purchased from Selleckchem.

Oligonucleotides. The lyophilized DNA sequences (Table 3), purchased from Eurogentec (Seraing, Belgium), were first diluted at 500 μM in deionized water (18.2 MΩ cm resistivity). The actual concentration of each DNA solution was determined after a dilution to 1 μM theoretical concentration through UV spectral analysis at 260 nm (after 5 min at 90 °C) with the molar extinction coefficient values provided by the manufacturer. Separated strands (FAM-TWJ-S1, TWJ-S1, TWJ-S2, TWJ-S3-TAMRA, and TWJ-S3) were subsequently diluted in a CacoK buffer (10 mM lithium cacodylate buffer plus 10 mM KCl/90 mM LiCl pH 7.2) at 2 μM for TWJ-screen and at 9 μM for PAGE experiments. For FRET-melting experiments, the higher-order DNA structures of both FAM-TWJ-TAMRA and ds26 were prepared by mixing 40 μL of the constitutive strand (500 μM) with 8 μL of a lithium cacodylate buffer solution (100 mM, pH 7.2), plus 8 μL of a KCl/LiCl solution (100/900 mM) and 24 μL of water. For ESI-MS analysis, the higher-order DNA structure was prepared by mixing 17 μL of TWJ (500 μM) with 17 μL of ammonium acetate buffer (1 M, pH 7.0) and 136 μL of water. The higher-order structures were folded according to two procedures: (a) for FAM-TWJ-TAMRA (FRET-melting) and TWJ (ESI-MS), solutions were heated (90 °C, 5 min), cooled on ice (FRET-melting) or to 25 °C gradually (ESI-MS), and then stored at least overnight (4 °C); and (b) for ds26, the solutions were heated (90 °C, 5 min), gradually cooled (65, 60, 55, 50, 40, and 30 °C (60 min per step), 25 °C (2 h)), and then stored overnight (4 °C).

TWJ-Screen Assay. Experiments are performed in a 96-well format plate (Greiner, F-bottom black) using a BMG Labtech ClarioStar equipped with FAM filters (λ_{ex} = 492 nm; λ_{em} = 516 nm) at 37 °C. Experiments are performed in CacoK buffer (10 mM lithium cacodylate plus 10 mM KCl/90 mM LiCl, pH 7.2, final volume: 100 μL per well) with 1 μM ligand (10 μL of 10 μM solution) and 0.2 μM DNA (stepwise addition of 10 μL of 2 μM solution of FAM-TWJ-S1, TWJ-S2, and TWJ-S3-TAMRA). The microplate is centrifuged quickly (30 s) and then placed into the ClarioStar. The FAM fluorescence is monitored upon gentle stirring at 37 °C every 5 min during 1 h. Final data are analyzed by using Excel (Microsoft Corp.) and OriginPro9 (OriginLab Corp.): the results are expressed as normalized fluorescence intensity (NFI) values collected at 60 min. The efficiency of ligands to fold TWJ is quantified by comparing the NFI of FAM-TWJ-S1 alone (defined as 100%) versus [FAM-TWJ-S1 + ligand] (for discarding unwarranted ligand's interaction with FAM-TWJ-S1) on the one hand and the NFI of the mixture M ([FAM-TWJ-S1 + TWJ-S2 + TWJ-S3-TAMRA]) versus [M + ligand] (that quantifies the TWJ folding per se) on the other hand. Reported NFI values are means of three experiments.

FRET-Melting Assay. Experiments are performed in a 96-well format plate (Agilent) using Agilent Stratagene Mx3005P equipped with FAM filters (λ_{ex} = 492 nm; λ_{em} = 516 nm) from 25 to 90 °C. Experiments are performed in CacoK buffer (10 mM lithium cacodylate plus 10 mM KCl/90 mM LiCl, pH 7.2, final volume: 100 μL per well) with 0.2 μM DNA (the labeled sequence FAM-TWJ-TAMRA), and 1 μM ligand (1 μL of 100 μM solution). The microplate is centrifuged quickly (10 s), gently stirred for 30 min at 25 °C, centrifuged quickly (10 s) again, and then placed into Mx3005P. After a first equilibration step (25 °C, 30 s), a stepwise increase of 1 °C every 30 s for 65 cycles to reach 90 °C was performed, and measurements were made after each cycle. Final data were analyzed with Excel and OriginPro9. The emission of FAM was normalized (0 to 1), and $T_{1/2}$ was defined as the temperature for which the normalized emission is 0.5; reported $\Delta T_{1/2}$ values are means of three experiments. Competitive experiments are performed similarly, that is, with labeled DNA (FAM-TWJ-TAMRA, 0.2 μM) in the presence of a ligand (1.0 μM, 5 mol equiv) and increasing amounts (3.0 and 10.0 μM, 15 and 50 mol equiv) of the unlabeled competitor ds26.

Polyacrylamide Gel Electrophoresis. Nondenaturing polyacrylamide gel electrophoresis (PAGE) was performed according to the protocol described by Malina et al.[22] in 15% polyacrylamide gel (prepared by mixing 6.8 mL of acrylamide (40%), 11.2 mL of TBE buffer, 180 μL of APS (10% w/v), and 18 μL of TEMED; 15 min polymerization). Samples were prepared in 18 μL (volume) comprising 15 μL of DNA or DNA/ligand mixtures plus 3 μL of DNA loading dye (6×). Each solution was prepared separately: TWJ-S1 alone (6 μM), [TWJ-S1 + TWJ-S2 + TWJ-S3] (or M) (6 μM), [M (6 μM) + 1 mol equiv ligand (6 μM)], [M (6 μM) + 2 mol equiv ligand (12 μM)], [M (6 μM) + 3 mol equiv ligand (18 μM)], [M (6 μM) + 5 mol equiv ligand (30 μM)], and [TWJ-S1 + TWJ-S2] (6 μM); the solutions were stirred for 1 h at 25 °C prior to the addition of 3 μL of DNA loading dye (6×). These mixes were stirred for 15 min at 25 °C (a period during which the gel is stacked at 7 W (150−180 V, 43−38 mA) in TBE buffer enriched with 100 mM NaCl, pH 8.3) prior to the loading of 12 μL per well of each solution and 1 h migration at 7 W. After the migration, gels were analyzed after a poststaining step (SYBR Gold solution, 1:10 000, 10 min, 25 °C under gentle agitation) with a UVP MultiDoc-It imaging system (λ_{ex} = 302 nm). Competitive PAGE experiments were performed according to a similar protocol but including FAM-TWJ-S1 (instead of the unlabeled TWJ-S1). Then, 15 μL of the following solutions was prepared: ds12 alone (Table 3) (252 μM-nt), M alone (252 μM-nt), [M (252 μM-nt) + 2 mol equiv ligand (12 μM)], [M (252 μM-nt) + 2 mol equiv ligand (12 μM) + 1 mol equiv ds12 (252 μM-nt)], [M (252 μM-nt) + 2 mol equiv ligand (12 μM) + 5 mol equiv ds12 (1260 μM-nt)], [M (252 μM-nt) + 2 mol equiv ligand (12 μM) + 10 mol equiv ds12 (2520 μM-nt)]. The solutions were stirred for 1 h at 25 °C prior to the addition of 3 μL of sucrose 48%. These mixes were stirred for 15 min at 25 °C prior to the loading of 12 μL per well of each solution and 50 min migration at 7 W. After the migration, gels were poststained (SYBRGold solution, 1:10 000) and imaged with the MultiDoc-It (λ_{ex} = 302 nm).

ESI-MS Analysis. Electrospray mass spectrometry experiments were performed on an LTQ Orbitrap XL (Thermo Scientific) spectrometer equipped with an Ion Max source and a HESI-II probe in the negative ion mode. TWJ and ds17 alone as well as the corresponding DNA/ligand mixtures (1:1 and 1:2 mol equiv) were prepared in 100 mM ammonium acetate buffer and equilibrated at 25 °C for 1 h. To obtain a stable electrospray signal, 20% methanol was added to the solution just before injection. The solutions were injected with a syringe pump at a flow rate of 5 μL min^{-1}. The full scan mass was recorded in the 600−4000 m/z range. The following tuning parameters were used: heater temperature = 50 °C, spray voltage = 4.0 kV, capillary temperature = 275 °C, tube lens = −160.00 (negative ion mode), and capillary voltage between −35.00 and −60.00 V. Quantification of the equilibrium affinity constants (K) of

DOI: 10.1021/acs.jmedchem.8b01978
J. Med. Chem. 2019, 62, 4456−4466

ligands for either TWJ or ds17 has been done according to the procedure described by Rosu et al.[39]

Competition Equilibrium Dialysis. The oligonucleotide solutions of TWJ and ds17 were prepared as 75 μM (base pair) concentration in 111 mM NaCl solution. These solutions were then heated at 90 °C for 5 min, cooled down slowly to 25 °C, and left at 4 °C overnight. For each dialysis experiment, four dialysis units were used (Slide-A-Lyzer MINI Dialysis Units, molecular weight cutoff: 3.5 kDa) that were previously washed with milli-Q water. Two of them were filled with 200 μL of TWJ DNA solution and the other two bags with 200 μL of the solution of duplex DNA ds17. Dialysis units were then placed into a beaker containing 200 mL of 2−2.5 μM solution of the tested ligand enriched with 111 mM NaCl, covered with parafilm and aluminum foil, and allowed to equilibrate for 24 h at room temperature. The solutions from each dialysis unit were then transferred to Eppendorf tubes. The content of each bag was then mixed with sodium dodecyl sulfate solution (10%) to reach a 1% SDS concentration (v/v). The concentrations of the free product in the dialysate solution and product concentrations in the dialysis bags were determined by fluorescence measurements using the molar extinction coefficients of the ligand (determined in the presence and absence of the detergent; see Tables 4 and 5, respectively), and finally, the apparent association constants (K_{app}) were calculated according to the formula:[40] K_{app} = [L-NA]/[NA][L], expressed in M^{-1}, in which [L-NA] is the concentration of the ligand bound to nucleic acid determined as a difference between the total ligand concentration inside the dialysis unit and the free ligand concentration (dialysate solution), [NA] is the concentration of free DNA calculated as a difference between the initial concentration of nucleic acid and [L-NA], and [L] is the free ligand concentration (dialysate solution).

Table 4. Extinction Coefficients of the Tested Ligands

ligand	excitation wavelength (nm)	emission wavelength (nm)	molar fluorescence extinction coefficient (mol^{-1} L^{-1} cm^{-1})
451	285	330	2.33×10^9
459	300	400	4.74×10^8
471	200	319	9.38×10^8

Table 5. Molar Fluorescent Extinction Coefficients of the Tested Ligands

ligand	excitation wavelength (nm)	emission wavelength (nm)	molar fluorescence extinction coefficient (mol^{-1} L^{-1} cm^{-1})
451	285	335	3.91×10^9
459	300	400	1.07×10^9
471	200	318	6.58×10^8

Cell Culture. MCF7 and MDA-MB-231 (breast adenocarcinoma) cells were routinely cultured in 75 cm^2 tissue culture flasks (Nunc) at 37 °C in a humidified, 5% CO_2 atmosphere in Dulbecco's modified Eagle's medium (DMEM) supplemented with 10% fetal bovine serum (FBS, Gibco) and a 1% penicillin−streptomycin (Pen−Strep, 5.0 units mL^{-1} Pen/5.0 μg mL^{-1} Strep, Gibco) mixture. The same culture conditions were used for BJ-hTERT, normal foreskin fibroblasts immortalized by hTERT transduction, except that the growth medium was a 4:1 mixture of DMEM and M199 medium supplemented with 15% FBS and Pen−Strep. Cells were subcultured twice a week using a standard protocol: the medium was first removed by aspiration; the cells were subsequently washed once with Dulbecco's phosphate-buffered saline, and 1.5 mL of a trypsin solution (0.25%, Gibco) was added. After 5 min at 37 °C, cells were manually harvested, and 500 μL of the solution of cells in the suspension was dispensed into three cell culture flasks containing 10 mL of DMEM medium (with 10% FBS and 1% Pen−Strep).

Cell Proliferation SRB Assay. The antiproliferative properties of the ligands were assessed through the sulforhodamine B (SRB) assay according to the protocols described by Vichai & Kirtikara and Skehan et al.[41,42] Cells were seeded in a 96-well plate (6000 cells per well) in 160 μL of growth medium for 24 h at 37 °C. Then, 40 μL of the ligand solution was added to reach the final concentration of the ligands between 500 and 0.05 μM or 50 and 0.005 μM and incubated for 72 h at 37 °C. After 72 h, the media was removed and the cells were fixed with a solution of trichloroacetic acid 10% (150 μL, 1 h at 4 °C). The supernatant was removed, and the fixed cells were washed with water and then dried. A 100 μL solution of SRB (0.2% in 1% acetic acid) was added into each well (except control wells); after 30 min, the supernatant was removed, the wells were washed three times with 150 μL of acetic acid (1%), and dried. After that, 150 μL of Tris base (10 mM) was added in each well, and the microplate was gently stirred for 5 min at 25 °C. Optical density (OD) values were determined at 530 nm. Final data were analyzed with Excel (Microsoft Corp.) and GraphPad 7.0 (Prism software): the OD_{530nm} was normalized (from 0 to 100; 0 for ligand untreated, SRB unstained cells and 100 for ligand untreated, SRB stained cells), and LD_{50} (lethal dose, defined as the concentration at which 50% of the cell growth inhibition is reached) was determined for a normalized OD_{530nm} of 50%; reported LD_{50} values are means of three experiments.

■ ASSOCIATED CONTENT

Supporting Information

The Supporting Information is available free of charge on the ACS Publications website at DOI: 10.1021/acs.jmedchem.8b01978.

ESI-MS evaluations of **451**, **459**, and **471** with both TWJ-DNA and ds-DNA (Figures S1−S3), SRB assays performed with MCF7 and MDA-MB-231 cells and camptothecin, and with BJ-hTERT and **451**, **459**, **471**, and camptothecin (Figure S4) and immunodetection experiments performed with MCF7 cells and **471** and camptothecin (Figure S5) (PDF)

Complete TWJ-screen results and the molecular formula strings (CSV)

Top ligand selection (XLSX)

■ AUTHOR INFORMATION

Corresponding Author

*E-mail: david.monchaud@cnrs.fr.

ORCID

Charles H. Devillers: 0000-0001-9078-7035
Anton Granzhan: 0000-0002-0424-0461
Murielle Chavarot-Kerlidou: 0000-0003-2709-3772
Bruno Therrien: 0000-0002-0388-2745
David Monchaud: 0000-0002-3056-9295

Funding

This project has received funding from the European Union's Horizon 2020 research and innovation program (grant agreement H2020-MSCA-IF-2016-750368), from the Agence Nationale de la Recherche (grant agreement ANR-17-CE17-0010-01), and IDEX Paris Saclay ("IDI 2016", ANR-11-IDEX-0003-02) and is also part of the project "Pharmacoimagerie & agents théranostiques" supported by the Université de Bourgogne and Conseil Régional de Bourgogne (PARI) and the European Union (PO FEDER-FSE Bourgogne 2014/2020 programs).

Notes

The authors declare no competing financial interest.

DOI: 10.1021/acs.jmedchem.8b01978
J. Med. Chem. 2019, 62, 4456−4466

■ ACKNOWLEDGMENTS

The authors thank Medicines for Malaria Venture for the Pathogen Box and the French National Chemical Library for the CNE, as well as R. A. Weinberg for the gift of the BJ-hTERT cell line.

■ ABBREVIATIONS

DNA, deoxyribonucleic acid; TWJ, three-way DNA junction; PAGE, polyacrylamide gel electrophoresis; FRET, fluorescence resonance energy transfer; ESI-MS, electrospray ionization mass spectrometry; SRB, sulforhodamine B; HTS, high-throughput screen; CNE, chimiothèque nationale essentielle; ICMUB, institut de chimie moléculaire de l'université de Bourgogne; FAM, fluorescein amidite; TAMRA, tetramethylrhodamine amidite; NFI, normalized FAM intensity; SDS, sodium dodecyl sulfate; LD, lethal dose; DDR, DNA damage response; DMEM, Dulbecco's modified Eagle medium; FBS, fetal bovine serum; OD, optical density

■ REFERENCES

(1) Zeman, M. K.; Cimprich, K. A. Causes and consequences of replication stress. *Nat. Cell Biol.* **2014**, *16*, 2−9.
(2) Técher, H.; Koundrioukoff, S.; Nicolas, A.; Debatisse, M. The impact of replication stress on replication dynamics and DNA damage in vertebrate cells. *Nat. Rev. Genet.* **2017**, *18*, 535−550.
(3) Gaillard, H.; García-Muse, T.; Aguilera, A. Replication stress and cancer. *Nat. Rev. Cancer* **2015**, *15*, 276−289.
(4) Dobbelstein, M.; Sørensen, C. S. Exploiting replicative stress to treat cancer. *Nat. Rev. Drug Discovery* **2015**, *14*, 405−423.
(5) Jackson, S. P.; Bartek, J. The DNA-damage response in human biology and disease. *Nature* **2009**, *461*, 1071−1078.
(6) Ciccia, A.; Elledge, S. J. The DNA damage response: making it safe to play with knives. *Mol. Cell* **2010**, *40*, 179−204.
(7) Rodriguez, R.; Miller, K. M. Unravelling the genomic targets of small molecules using high-throughput sequencing. *Nat. Rev. Genet.* **2014**, *15*, 783−796.
(8) Helleday, T.; Petermann, E.; Lundin, C.; Hodgson, B.; Sharma, R. A. DNA repair pathways as targets for cancer therapy. *Nat. Rev. Cancer* **2008**, *8*, 193−204.
(9) Mirkin, E. V.; Mirkin, S. M. Replication fork stalling at natural impediments. *Microbiol. Mol. Biol. Rev.* **2007**, *71*, 13−35.
(10) Zhao, J.; Bacolla, A.; Wang, G.; Vasquez, K. M. Non-B DNA structure-induced genetic instability and evolution. *Cell. Mol. Life Sci.* **2010**, *67*, 43−62.
(11) Caruthers, J. M.; McKay, D. B. Helicase structure and mechanism. *Curr. Opin. Struct. Biol.* **2002**, *12*, 123−133.
(12) Zimmer, J.; Tacconi, E. M.; Folio, C.; Badie, S.; Porru, M.; Klare, K.; Tumiati, M.; Markkanen, E.; Halder, S.; Ryan, A.; et al. Targeting BRCA1 and BRCA2 deficiencies with G-quadruplex-interacting compounds. *Mol. Cell* **2016**, *61*, 449−460.
(13) Xu, H.; Di Antonio, M.; McKinney, S.; Mathew, V.; Ho, B.; O'Neil, N. J.; Dos Santos, N.; Silvester, J.; Wei, V.; Garcia, J.; et al. CX-5461 is a DNA G-quadruplex stabilizer with selective lethality in BRCA1/2 deficient tumours. *Nat. Commun.* **2017**, *8*, No. 14432.
(14) Lemmens, B.; Van Schendel, R.; Tijsterman, M. Mutagenic consequences of a single G-quadruplex demonstrate mitotic inheritance of DNA replication fork barriers. *Nat. Commun.* **2015**, *6*, No. 8909.
(15) Bochman, M. L.; Paeschke, K.; Zakian, V. A. DNA secondary structures: stability and function of G-quadruplex structures. *Nat. Rev. Genet.* **2012**, *13*, 770−780.
(16) Hänsel-Hertsch, R.; Di Antonio, M.; Balasubramanian, S. DNA G-quadruplexes in the human genome: detection, functions and therapeutic potential. *Nat. Rev. Mol. Cell Biol.* **2017**, *18*, 279.
(17) Vuong, S.; Stefan, L.; Lejault, P.; Rousselin, Y.; Denat, F.; Monchaud, D. Identifying three-way DNA junction-specific small-molecules. *Biochimie* **2012**, *94*, 442−450.
(18) Novotna, J.; Laguerre, A.; Granzhan, A.; Pirrotta, M.; Teulade-Fichou, M.-P.; Monchaud, D. Cationic azacryptands as selective three-way DNA junction binding agents. *Org. Biomol. Chem.* **2015**, *13*, 215−222.
(19) Guyon, L.; Pirrotta, M.; Duskova, K.; Granzhan, A.; Teulade-Fichou, M.-P.; Monchaud, D. TWJ-Screen: an isothermal screening assay to assess ligand/DNA junction interactions in vitro. *Nucleic Acids Res.* **2018**, *46*, No. e16.
(20) Oleksi, A.; Blanco, A. G.; Boer, R.; Usón, I.; Aymamí, J.; Rodger, A.; Hannon, M. J.; Coll, M. Molecular recognition of a three-way DNA junction by a metallosupramolecular helicate. *Angew. Chem., Int. Ed.* **2006**, *45*, 1227−1231.
(21) Cerasino, L.; Hannon, M. J.; Sletten, E. DNA three-way junction with a dinuclear iron (II) supramolecular helicate at the center: A NMR structural study. *Inorg. Chem.* **2007**, *46*, 6245−6251.
(22) Malina, J.; Hannon, M. J.; Brabec, V. Recognition of DNA three-way junctions by metallosupramolecular cylinders: gel electrophoresis studies. *Chem. Eur. J.* **2007**, *13*, 3871−3877.
(23) Hotze, A. C.; Hodges, N. J.; Hayden, R. E.; Sanchez-Cano, C.; Paines, C.; Male, N.; Tse, M.-K.; Bunce, C. M.; Chipman, J. K.; Hannon, M. J. Supramolecular iron cylinder with unprecedented DNA binding is a potent cytostatic and apoptotic agent without exhibiting genotoxicity. *Chem. Biol.* **2008**, *15*, 1258−1267.
(24) Boer, D. R.; Kerckhoffs, J. M.; Parajo, Y.; Pascu, M.; Usón, I.; Lincoln, P.; Hannon, M. J.; Coll, M. Self-Assembly of functionalizable two-component 3D DNA arrays through the induced formation of DNA three-way-Junction branch points by supramolecular cylinders. *Angew. Chem., Int. Ed.* **2010**, *49*, 2336−2339.
(25) Barros, S. A.; Chenoweth, D. M. Recognition of nucleic acid junctions using triptycene-based molecules. *Angew. Chem., Int. Ed.* **2014**, *53*, 13746−13750.
(26) Barros, S. A.; Chenoweth, D. M. Triptycene-based small molecules modulate (CAG)·(CTG) repeat junctions. *Chem. Sci.* **2015**, *6*, 4752−4755.
(27) Yang, Z.; Chen, Y.; Li, G.; Tian, Z.; Zhao, L.; Wu, X.; Ma, Q.; Liu, M.; Yang, P. Supramolecular recognition of three way junctions DNA by a cationic calix [3] carbazole. *Chem. Eur. J.* **2018**, *24*, 6087−6093.
(28) Van Voorhis, W. C.; Adams, J. H.; et al. Open source drug discovery with the malaria box compound collection for neglected diseases and beyond. *PLoS Pathog.* **2016**, *12*, No. e1005763.
(29) Wells, T. N.; Willis, P.; Burrows, J. N.; van Huijsduijnen, R. H. Open data in drug discovery and development: lessons from malaria. *Nat. Rev. Drug Discovery* **2016**, *15*, 661−662.
(30) Mahuteau-Betzer, F. The french national compound library: advances and future prospects. *Med. Sci.* **2015**, *31*, 417−422.
(31) Kadrmas, J. L.; Ravin, A. J.; Leontis, N. B. Relative stabilities of DNA three-way, four-way and five-way junctions (multi-helix junction loops): unpaired nucleotides can be stabilizing or destabilizing. *Nucleic Acids Res.* **1995**, *23*, 2212−2222.
(32) Granzhan, A.; Monchaud, D.; Saettel, N.; Guédin, A.; Mergny, J.-L.; Teulade-Fichou, M.-P. "One ring to bind them all"—Part II: Identification of promising G-quadruplex ligands by screening of cyclophane-type macrocycles. *J. Nucleic Acids* **2010**, *2010*, No. 460561.
(33) Freudenreich, J.; Barry, N. P.; Süss-Fink, G.; Therrien, B. Permanent encapsulation or host−guest behavior of aromatic molecules in hexanuclear arene ruthenium prisms. *Eur. J. Inorg. Chem.* **2010**, *2010*, 2400−2405.
(34) Gaschard, M.; Nehzat, F.; Cheminel, T.; Therrien, B. Arene ruthenium metalla-assemblies with anthracene moieties for PDT applications. *Inorganics* **2018**, *6*, 97.
(35) Stefan, L.; Bertrand, B.; Richard, P.; Le Gendre, P.; Denat, F.; Picquet, M.; Monchaud, D. Assessing the differential affinity of small molecules for noncanonical DNA structures. *ChemBioChem* **2012**, *13*, 1905−1912.

DOI: 10.1021/acs.jmedchem.8b01978
J. Med. Chem. 2019, 62, 4456−4466

(36) Laguerre, A.; Chang, Y.; Pirrotta, M.; Desbois, N.; Gros, C. P.; Lesniewska, E.; Monchaud, D. Surface-promoted aggregation of amphiphilic quadruplex ligands drives their selectivity for alternative DNA structures. *Org. Biomol. Chem.* **2015**, *13*, 7034−7039.
(37) de Robillard, G.; Makni, O.; Cattey, H.; Andrieu, J.; Devillers, C. H. Towards sustainable synthesis of pyren-1-yl azoliums via electrochemical oxidative C−N coupling. *Green. Chem.* **2015**, *17*, 4669−4679.
(38) Gabelica, V.; Rosu, F.; De Pauw, E. A simple method to determine electrospray response factors of noncovalent complexes. *Anal. Chem.* **2009**, *81*, 6708−6715.
(39) Rosu, F.; Gabelica, V.; Houssier, C.; De Pauw, E. Determination of affinity, stoichiometry and sequence selectivity of minor groove binder complexes with double-stranded oligodeoxynucleotides by electrospray ionization mass spectrometry. *Nucleic Acids Res.* **2002**, *30*, No. e82.
(40) Ragazzon, P. A.; Garbett, N. C.; Chaires, J. B. Competition dialysis: a method for the study of structural selective nucleic acid binding. *Methods* **2007**, *42*, 173−182.
(41) Vichai, V.; Kirtikara, K. Sulforhodamine B colorimetric assay for cytotoxicity screening. *Nat. Protoc.* **2006**, *1*, 1112−1116.
(42) Skehan, P.; Storeng, R.; Scudiero, D.; Monks, A.; McMahon, J.; Vistica, D.; Warren, J. T.; Bokesch, H.; Kenney, S.; Boyd, M. R. New colorimetric cytotoxicity assay for anticancer-drug screening. *JNCI, J. Natl. Cancer Inst.* **1990**, *82*, 1107−1112.
(43) Pommier, Y. Topoisomerase I inhibitors: camptothecins and beyond. *Nat. Rev. Cancer* **2006**, *6*, 789−802.
(44) Hahn, W. C.; Counter, C. M.; Lundberg, A. S.; Beijersbergen, R. L.; Brooks, M. W.; Weinberg, R. A. Creation of human tumour cells with defined genetic elements. *Nature* **1999**, *400*, 464−468.
(45) Bonner, W. M.; Redon, C. E.; Dickey, J. S.; Nakamura, A. J.; Sedelnikova, O. A.; Solier, S.; Pommier, Y. γH2AX and cancer. *Nat. Rev. Cancer* **2008**, *8*, 957−967.
(46) O'Connor, M. J. Targeting the DNA damage response in cancer. *Mol. Cell* **2015**, *60*, 547−560.
(47) Kotera, N.; Poyer, F.; Granzhan, A.; Teulade-Fichou, M.-P. Efficient inhibition of human AP endonuclease 1 (APE1) via substrate masking by abasic site-binding macrocyclic ligands. *Chem. Commun.* **2015**, *51*, 15948−15951.
(48) Caron, C.; Duong, X. N. T.; Guillot, R.; Bombard, S.; Granzhan, A. Interaction of functionalized naphthalenophanes with abasic sites in DNA: DNA cleavage, DNA cleavage inhibition, and formation of ligand−DNA adducts. *Chem. Eur. J.* **2019**, *25*, 1949−1962.

DOI: 10.1021/acs.jmedchem.8b01978
J. Med. Chem. 2019, 62, 4456−4466